4. Materials

As explained already this treatise is part of a common project of two working groups. All samples were prepared by Prof. Keune's group and were studied among others by using x-ray diffraction and CEMS measurements. Hence, some basic information needed for understanding my results will briefly be reviewed. More details about the sample preparation and structural studies can be found in the doctoral thesis of J. Tappert [Tapp98]. In the following the physical properties of Fe, Tb and Y, the sample preparation and the experimental procedures, MOKE, SQUID and torque measurements, will be explained. Finally, structural peculiarities of Fe/Tb MLs will briefly be summarized.

4.1. Physical properties of Fe, Tb and Y

Chemically pure metallic iron, Fe, crystallizes below 1179 K in a stable body centred cubic (bcc) structure (α-Fe) with a density of 7.873 g/cm³ [Kitt86]. The atomic radius and the lattice constant amount to 0.126 nm [Kitt86] and a = 0.2866 nm at RT [Cull59], respectively. The transition metal Fe has an electronic configuration of $3d^6 4s^2$ and is ferromagnetically ordered below T_C = 1043 K [Kitt86]. The magnetic moment μ_{Fe} = 2.218 μ_B/atom at T = 0 K, corresponding to a saturation magnetisation of 1.746 MA/m [Kitt86], is primarily due to that of the 3d electrons. This leads to the consequence that 3d transition metals show a very small crystalline magnetic anisotropy.

Terbium, Tb, chemically belongs to 3rd subsidiary group (lanthanides) of the periodic system of elements (PSE). Its electron configuration is $4f^8 5s^2 5p^6 5d^1 6s^2$ [Kitt86]. The 4f orbital is well screened through the outer orbitals so that the chemical peculiarities of RE elements are determined by $5d^1 6s^2$ orbitals. This leads to nearly identical chemical properties of all RE elements. The density amounts to 8.25 g/cm³. At RT Tb crystallizes in the hexagonal close packed structure (hcp). The lattice constants are a = 0.3604 nm and c = 0.5698 nm [Elli72]. The atomic radius lies at 0.173 nm [Elli72]. The magnetic behavior of Tb is determined by the 4f orbital. In particular, the orbital moment in RE elements is not quenched and contributes to total magnetic moment. The magnetic moment, μ_{Tb} = 9.72 μ_B/atom at T = 0 K [Elli72], is equivalent to that of the free atom and is determined by Hund's rules. There are two magnetic

phase transitions. Above the Néel temperature, $T_N = 230.2$ K, Tb is paramagnetic. Between T_N and $T_C = 219.6$ K an antiferromagnetic phase exists, where a helimagnetic structure is found. In this case all magnetic moments lie parallel in the hexagonal basal plane and each moment rotates by an angle from one layer to the following one perpendicular to the c axis. The turn angle depends on the temperature and lies between 43 and 26° [Coqb77]. Below $T_C = 219.6$ K all moments lie parallel within the hexagonal basal plane [Elli72].

The magnetic interaction between TM and RE elements is determined by indirect exchange between the 3d electrons of the TM and the 4f electrons of the RE via the 5d electrons [Ball92]. The exchange integral between 3d electron of TM and 5d electron of RE element is negative so that spins turn antiparallel. The 5d electrons again overlap with the 4f electron. According to Hund's rules the orbital moment orients parallel to the spin moment so that the net moment of the 4f electrons aligns antiparallel to the 3d electron of TM when the 4f orbital is filled more than half. This applies to the heavy RE elements Gd, Tb, Dy, Ho, Er, Tm, Yb and Lu [Camp72, Ball92]. This leads to a ferrimagnetic behavior, where the sublattice magnetizations of Fe and Tb show different temperature dependencies. This is why at a certain temperature, the compensation temperature T_{comp}, the total magnetization cancels out.

In the light RE elements, Ce, Pr, Nd, Pm, Sm and Eu, the orbital moment aligns antiparallel to the spin moment so that moment of the 4f electron orients parallel to the 3d electrons of TM. Thus TM-RE alloys reveal ferromagnetic behavior [Hans90, Dava93].

Yttrium, Y, belongs chemically to the group of the 4d TM-metals within the PSE. But Yttrium shows similar physical properties to those of Tb. E. g., it has the same hcp structure, similar electronegativity and lattice constant. Its electron configuration is $4d^1 5s^2$ [Kitt86]. In contrast to Tb, Yttrium does not contain 4f moments. That is why Yttrium is an appropriate ML component allowing us to study the chemical and structural properties of the RE subsystem without exerting any magnetic interactions.

4.2. Preparation

All Fe/Tb MLs were prepared by alternating thermal evaporation of high-purity metals (Fe: 99.9985 at. % purity; Tb: 99.99 at. % purity ; Ag: 99.99 at. % purity) in a UHV system on (100) oriented Si substrates. The materials were evaporated from W crucibles for Tb and Y or from alumina crucibles for Fe and Ag in resistively heated Knudsen cell-type ovens. Each of these ovens was surrounded by Mo heat shields, which were cooled by LN_2 or water. The distance between the oven openings and the substrate was about 400 mm. The pressure was kept below $5 \cdot 10^{-9}$ mbar during evaporation. The deposition rates and layer thickness were controlled by calibrated quartz microbalances located close to the substrate position. The deposition rates amount to 0.01 - 0.03 nm/s for Fe, Tb and Y and 0.1 nm/s for Ag, respectively. Different thicknesses of the individual layers were chosen in the following four series of MLs:

(i) different Fe thicknesses, t_{Fe} = 1.0 - 5.0 nm, at constant Tb thickness, t_{Tb} = 1.9 nm in MLs with 19 Fe/Tb bilayers and one additional top layer of Fe with t_{Fe},

(ii) samples with diamagnetic Y layers: t_{Fe} = 5.0 nm and t_{Tb} = 2.6 nm, and t_{Fe} = 5.0 nm, t_{Tb} = 1.4 nm and t_Y = 1.2 nm (here t_{RE} = 2.6 nm remains), respectively, in MLs with n = 10 Fe/RE bilayers,

(iii) samples with diamagnetic Ag layers: t_{Fe} = 3.5 nm, t_{Tb} = 1.4 nm and t_{Ag} = 5.0 nm and n = 10,

(iv) samples with n = 1, 2, 3 and 10 periods of Fe/Tb bilayers with t_{Fe} = 3.5 nm and t_{Tb} = 1.4 nm. The deposition rates amount to about 0.0005 nm/s for Fe and Tb.

In the case (i) the growing temperature of the layer, T_s, was varied. Two values, low T_s = 150 (LT) and high T_s = 300 K (HT), were chosen in order to study influence of the preparation temperature on the morphological and magnetic properties of the interfaces. In all other cases the samples were deposited at T = 300 K.

For the case of α-Fe/Tb MLs it is well-known that the two interfaces of the individual Fe layers, bottom (Fe-on-Tb) and top (Tb-on-Fe), have different properties [Scho94a, Tapp94, Rich96a]. In order to investigate the influence of the individual interfaces either the top or the bottom layers adjacent to the Fe layers were replaced by diamagnetic Yttrium and Ag blocking layers, respectively. In the following S_j, j = 1, 2, 3, denote ML samples where either the top (j = 1) or the bottom (j = 2) or none of the RE layers (j = 3) adjacent to the Fe ones is replaced by S layers, where S = Y and Ag (Fig. 4.1).
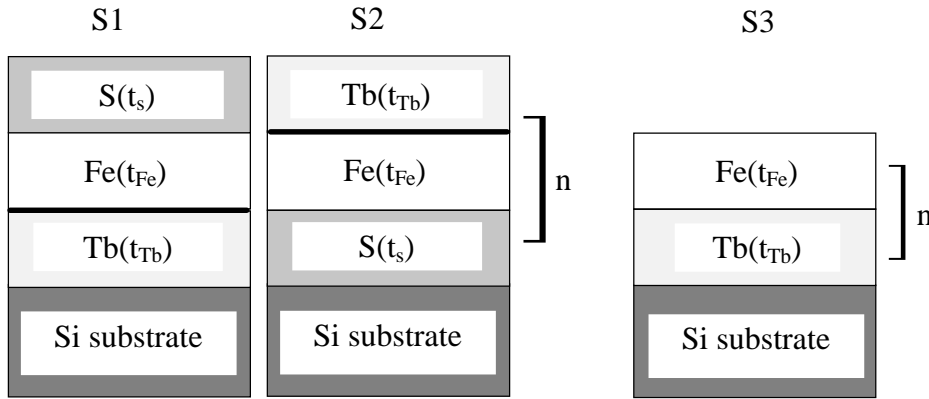
Fig. 4.1: Layer sequences of the MLs S_j, j = 1, 2, 3, including Fe and Tb layers with t_{Fe} and t_{Tb}, and diamagnetic blocking layers S (=Y or Ag) with thicknesses t_S and n = 10 periods of bi- and trilayers, respectively.

4.3. Experimental procedures

<u>MOKE:</u>

The samples are investigated by using the polar MOKE at wavelengths $275 \leq \lambda \leq 900$ nm and temperatures $50 \leq T \leq 300$ K in applied field magnetic fields $|H| \leq 4.8$ MA/m (see Chap. 3). In the following MOKE studies we restrict ourselves to the Kerr ellipticity, ε_K, in order to avoid cumbersome corrections of the Kerr rotation, θ_K, for the Faraday effect, θ_F, of the cryostat window. If linearly polarized light is transmitted through a medium under the influence of a magnetic field H parallel to the direction of propagation, the plane of polarization is rotated. This is known as the Faraday effect [Benn64], which occurs in the window of the Kerr polarimeter. For light of a given wavelength, the magnitude of the rotation is proportional to the magnetic field H and given by [Benn64]

$$\theta_F = V t_w H, \tag{4.1}$$

where V is the Verdet constant [Jenk50] and t_W is thickness of the window glass.

This is corroborated by measurements of the polar Kerr rotation, θ_K, on a Si substrate at RT and at different wavelengths, $\lambda = 300$ (●) and 700 nm (○), as shown in Fig. 4.2. Only very small diamagnetic contributions at H = 1.6 MA/m, θ_K = -0.15° and -0.04° at $\lambda = 300$ and 700 nm, respectively, were reported. Hence, the θ_K curves measured primarily represent the Faraday rotation of the window characterized by the wavelength dependent slope of the θ_K curves, $d\theta_K/dH$. Since the transparent quartz glass window does not exhibit Faraday ellipticity the resulting ε_K curve measured at RT and at $\lambda = 700$ nm (■) merely shows the Kerr ellipticity of Si. Obviously it is fluctuating by noise signals of ±0.01° around $\varepsilon_K \approx 0$.
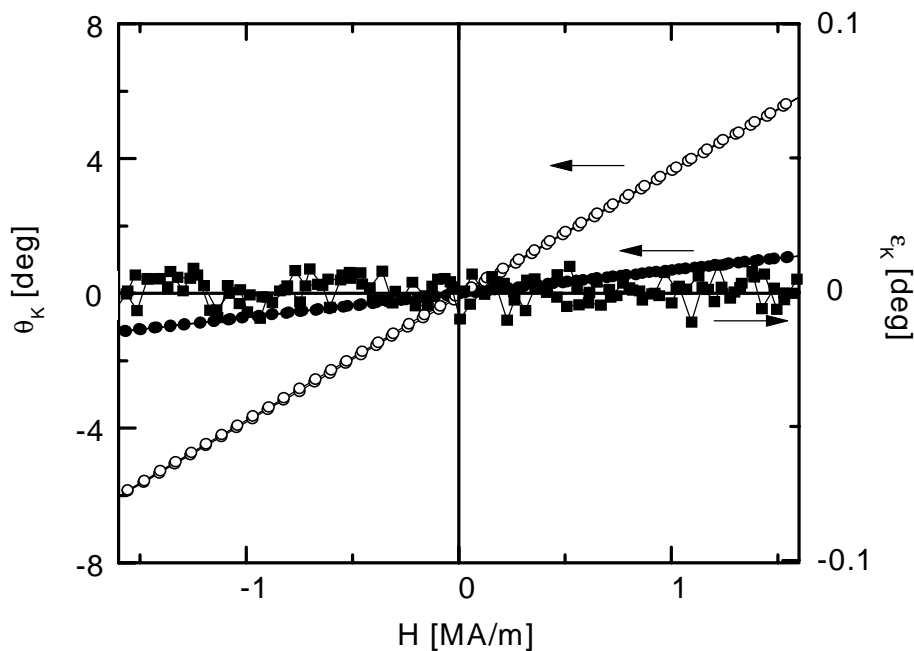

Fig. 4.2: Apparent polar Kerr rotation, θ_K (●, ○), and ellipticity, ε_K (■), curves of a Si substrate measured at RT and at wavelengths, $\lambda = 300$ (○) and 700 nm (●, ■) through a quartz glass window of thickness $t_W = 3.175$ mm.

In principle the θ_K curves measured can be corrected by the Verdet constant of the window material. It can be calculated by using the slopes of the θ_K curves in Fig. 4.2 which yields via Eq. (4. 1) the values V($\lambda = 300$ (700) nm) = $5.85 \cdot 10^{-4}$($1.11 \cdot 10^{-4}$) [°/A] in agreement with literature [Land62]. Note that an effective thickness of $2t_W$ has to be inserted into Eq. (4. 1) as a result of the retro-reflection. In practice, however, calibration measurements are not sufficiently exact in order to subtract the Faraday rotation from the Kerr rotation curves. θ_F is

also sensitive to ill-controlled measuring conditions, e. g. with respect to the incident angle φ of the light which actually does not vanish even in the polar geometry (φ = 3 ··· 5°).

SQUID magnetometry:

The magnetization reversal of the samples is measured by means of a Superconducting Quantum Interference Device (SQUID) magnetometer (Quantum Design MPMS-55) with the magnetic field either perpendicular (polar) or parallel (in-plane) to the sample plane at temperatures $5 \leq T \leq 300$ K and magnetic fields $|H| \leq 4$ MA/m. Small samples with sizes of about 3 x 3 mm² are cut of the prepared samples and stuck on the sample holder (Quantum Design) by using two-component glue „UHU plus". The sample holder consisted of a special Cu-Al alloy, which yields a diamagnetic contribution to the total magnetization. Hence, all SQUID curves were corrected by substrate signals containing contributions of the sample holder, glue and the Si substrate. Fig. 4.3 shows the SQUID magnetization curves, m(H), of a
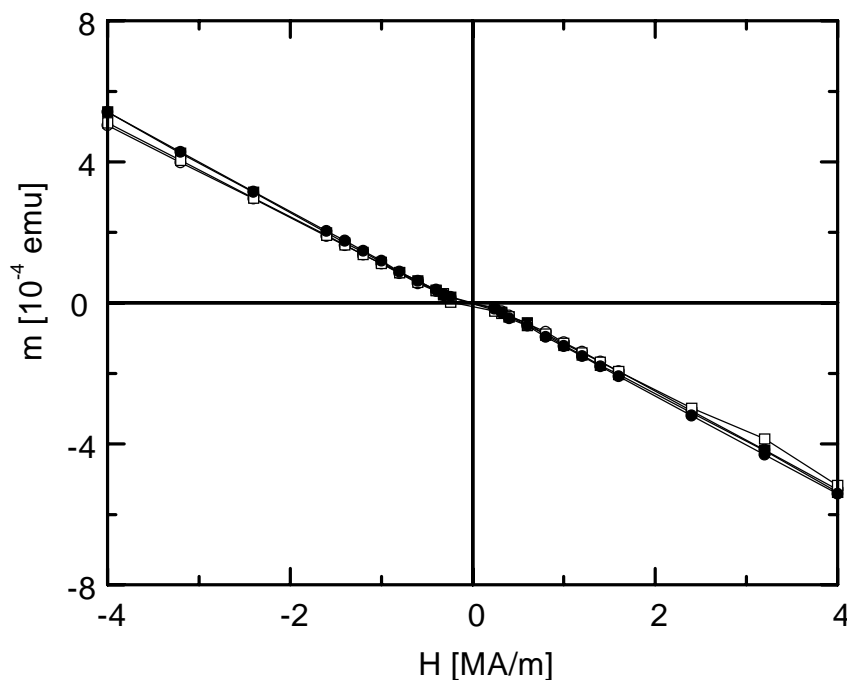

Fig. 4.3: SQUID magnetization measurements on a Si substrate with a mass of (7.77 ± 0.01) mg at different temperatures, T = 300 (●, ○) and 50 K (■, □), and in both polar (solid symbols) and in-plane (open symbols) geometries (see text).

Si substrate with a mass of (7.77 ± 0.01)mg determined by a microbalance (Sartorius). They primarily indicate nearly temperature independent diamagnetic behavior of the substrate at T ≥ 50 K except for small paramagnetic contributions at very low field strengths $|H| \leq 0.2$ MA/m. They give rise to an increase of the slope, dm/dH, and are probably caused by paramagnetic impurities in the sample holder and/or the glue.

Torque magnetometry:

Torque magnetometry has been carried out in the Institut für Physikalische Hochtechnologie at Jena in order to determine anisotropy constants. Torque curves (TCs) were obtained in the temperature range 15 K ≤ T ≤ RT as a function of the angle α between the applied field **H** and an arbitrary direction **e** within the film plane with an applied field of 0.72 MA/m (Fig. 4.4). The film plane is oriented perpendicularly to the plane of field-rotation. The torque τ lies perpendicularly to the both field **H** and the film normal **ñ** and is measured in a non-compensation mode while sweeping the applied field at intervals of Δα = 2° from α = 0 to 360° and back from α = 360 to 0° (counter-clockwise and clockwise, respectively; see Fig. 4.4).
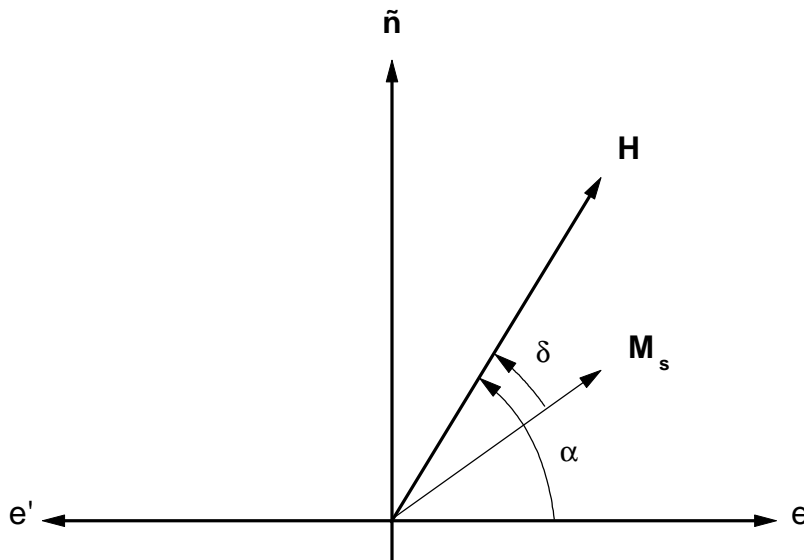
*Fig. 4.4: Geometry of the torque measurements, where **H** = applied field, **M**$_S$ = spontaneous magnetization, **ñ** = film normal, α = ∡(**e**, **H**), δ = ∡(**M**$_S$, **H**) and **ee'** = cross section of the film plane perpendicular to the field-rotation plane containing **H** and **ñ**.*

4.4. Structural peculiarities

The structure of the Fe layers in the Fe/Tb MLs is influenced by different factors, not only by the preparation conditions but also by the single layer thickness [Sato87b, Dufo91, Land91, Fnid93]. When depositing of Fe on Tb layers the Fe layer first grows amorphous up to a critical Fe thickness, t_{Fe}^{cr}. Above this the Fe layer crystallizes into the bcc α-phase except for a transition region of about 2 - 3 atomic layers [Land91]. Here, the crystallization process does not occur completely, because part of the iron remains amorphous at the interfaces due to large lattice mismatch between Fe and Tb (different atomic radii and crystal structures, see Chap. 4.1.).

The transition of the Fe layers from the amorphous to the crystalline structure strongly depends on the layer growing temperature [Dufo91, Land91] and deposition technique [Sato87b, Dufo91, Fnid93]. The critical Fe thickness at evaporation in UHV at RT lies between 2.0 and 2.5 nm [Dufo91, Land91] whereas it is considerably smaller at sputtering and amounts to $t_{Fe}^{cr} \approx 0.8$ nm [Sato87b] or 1.5 nm [Shan88]. This thickness-dependent crystallization is caused by the different structural parameters. This is corroborated by a comparison of different systems prepared under nearly the same conditions, e. g. evaporation in UHV at RT. Resistance measurements on Fe/Er and Fe/Tb [Dufo91], CEMS studies on Fe/Y and Fe/Gd [Land91], respectively, show similar critical thicknesses, t_{Fe}^{cr} of 2.0 - 2.5 nm, whereas t_{Fe}^{cr} for Fe/Mg is considerably smaller than that for TM/RE MLs and amounts to 1.2 nm although Mg has same hcp structure as the RE elements, where the atomic radius of Mg is smaller than that of RE elements [Kawa86].